

Cluster-CAM: Cluster-Weighted Visual Interpretation of CNNs' Decision in Image Classification

Zhenpeng Feng^a, Hongbing Ji^{a,*}, Miloš Daković^b, Xiyang Cui^a, Mingzhe Zhu^a and Ljubiša Stanković^b

^aSchool of Electronic Engineering, Xidian University, Xi'an, China

^bFaculty of Electrical Engineering, University of Montenegro, Podgorica, Montenegro

ARTICLE INFO

Keywords:

keywords-1 explainable artificial intelligence
keywords-2 class activation mapping
keywords-3 clustering algorithm
keywords-4 image classification

ABSTRACT

Despite the tremendous success of convolutional neural networks (CNNs) in computer vision, the mechanism of CNNs still lacks clear interpretation. Currently, class activation mapping (CAM), a famous visualization technique to interpret CNN's decision, has drawn increasing attention. Gradient-based CAMs are efficient while the performance is heavily affected by gradient vanishing and exploding. In contrast, gradient-free CAMs can avoid computing gradients to produce more understandable results. However, existing gradient-free CAMs are quite time-consuming because hundreds of forward interference per image are required. In this paper, we proposed Cluster-CAM, an effective and efficient gradient-free CNN interpretation algorithm. Cluster-CAM can significantly reduce the times of forward propagation by splitting the feature maps into clusters in an unsupervised manner. Furthermore, we propose an artful strategy to forge a cognition-base map and cognition-scissors from clustered feature maps. The final saliency heatmap will be computed by merging the above cognition maps. Qualitative results conspicuously show that Cluster-CAM can produce heatmaps where the highlighted regions match the human's cognition more precisely than existing CAMs. The quantitative evaluation further demonstrates the superiority of Cluster-CAM in both effectiveness and efficiency.

1. Introduction

Convolutional neural networks (CNNs) have provided a basis for numerous remarkable achievements in various computer vision tasks like, for example, image classification [9, 8, 27, 13], object detection [19, 43, 1, 12], and semantic segmentation [14, 11, 3]. Despite CNNs' extraordinary performance, they still lack a clear interpretation of the inner mechanism [10, 42, 21]. This lack of transparency can indeed be a disqualifying factor in some peculiar scenarios where mistakes in interpretation can jeopardize human life and health, like in medical image processing or autonomous vehicles [20, 38, 34, 32]. Therefore, it is highly desirable to find a way to understand and explain what exactly CNNs have learned during the training process [26, 31, 16].

Recently, Class Activation Mapping (CAM), a visual interpretation technique, has drawn increasing attention [30, 33]. CAM aims at highlighting saliency regions of an input image for CNN's decision using a linearly weighted combination of feature maps. Vanilla CAM directly utilizes the weight of each feature map after global average pooling (GAP) corresponding to the target class, so it is only available for CNNs with GAP [40]. To further extend CAM to more complex CNN structures, numerous modified CAMs are proposed and they can be broadly categorized as: 1) gradient-based CAMs, and 2) gradient-free CAMs. Gradient-based CAMs (e.g. Grad-CAM [23], Grad-CAM++ [2], SmoothCAM++ [17], XGrad-CAM [7] etc.) define the weights of each feature map using the average of partial gradient of the predicted score with respect to the feature maps. Gradient-based CAMs

are usually computed efficiently. However, their weights lack reasonable explanation and are easily impacted by gradient exploding or vanishing. To address this limitation, some gradient-free CAMs are proposed. They define an intuitive impact of each feature map on the predicted score instead of using the gradient. Examples of gradient-free CAMs are the Ablation CAM [18] and the Score-CAM [35]. Gradient-free CAMs can provide a more explainable weight definition than gradient-based CAMs in most cases. Fig. 1 shows the saliency heatmaps produced by several aforementioned CAMs.

Although gradient-free CAMs define the weights more reasonably, they are usually very time-consuming since hundreds of forward propagations per image are required. To improve the efficiency of gradient-free CAMs, Q. Zhang et al. proposed Group-CAM where feature maps are split into several groups [37]. In this case, only several forward propagations are needed in computing the weights. Nonetheless, the feature maps are split without any regulation in the Group-CAM. Actually, various feature maps have learned different semantic concepts relevant/irrelevant to the object. Therefore, the feature maps should be split into groups/clusters. Those with similar semantics should be assigned to the same group. Z. Feng et al. proposed SC-SM CAM using spectral clustering to accomplish this goal, particularly for synthetic aperture radar (SAR) images [5]. However, no further analysis or modification of weights is mentioned in the SC-SM CAM [6, 5].

In this paper, we propose a Cluster-CAM, an effective and efficient gradient-free CAM, based on unsupervised clustering. In Cluster-CAM, an unsupervised clustering technique, K-means/spectral clustering is adopted to split feature maps into several clusters. Subsequently, we provide an artful strat-

*Corresponding author: Hongbing Ji

✉ hbji@xidian.edu.cn (Hongbing Ji)
ORCID(s):

egy to merge those feature maps into a cognition-base map and a cognition-scissors map which will be combined as the final salience heatmap. The highlights of this paper are as follows:

- We propose a Cluster-CAM, as the first attempt to provide a cluster-weighted CAM framework via unsupervised clustering based on optical images.
- We provide a novel and artful weight-forming strategy to merge the cognition-base map and cognition-scissors map. These two maps greatly match the human's cognition and intuition, thus the weights are completely reasonable and understandable.
- Cluster-CAM is effective and efficient, which outperforms existing gradient-free CAMs in performance in most cases with significantly lower computing costs.

The rest of this paper is organized as follows. Section 2 introduces the basic knowledge of various CAMs. Section 3 elaborates on how to generate salience heatmaps by Cluster-CAM. In Section 4, various experiments are implemented to demonstrate the validity of Cluster-CAM and further analyze the experimental results from various aspects. Section 5 concludes this paper.

2. Related Work

As discussed in Section 1, the key issue in interpreting CNN's decision is to explain what the neural network learned to finish a reasonable inference [42, 10]. To visualize what CNN focuses on the input image, numerous interpretation algorithms are proposed [36, 24, 40, 39], among which Class Activation Mapping draws the most increasing attention due to its simplicity and good performance.

Vanilla CAM: B. Zhou et al. firstly proposed the vanilla CAM to produce a salience heatmap by a linearly weighted combination of feature maps, \mathbf{F}_n , with elements $F_n(i, j)$, $n = 1, 2, \dots, N$, at the target convolutional layer before classification [40]

$$M_c(i, j) = \sum_n \alpha_n^c F_n(i, j) \quad (1)$$

$$S_c = \sum_n \omega_n^c \sum_{i,j} F_n(i, j) = \sum_n \alpha_n^c \sum_{i,j} F_n(i, j), \quad (2)$$

where $M_c(i, j)$ is a heat-map and S_c denotes the predicted score for the target class c . Thus, α^c are defined by the weights, ω^c , of each feature map corresponding to c -th unit in the classification layer. Therefore, CAM is only available with CNNs with global-average pooling following the last convolutional layer. To extend CAM to all CNNs, many modified CAMs are further proposed by manipulating the definition of weights, which are generally categorized as: 1) gradient-based CAMs; 2) gradient-free CAMs.

2.1. Gradient-based Class Activation Mapping

Gradient-based CAM: Selvaraju et al. proposed Grad-CAM to visualize any classification CNN architectures by weighting the feature maps in a certain convolutional layer with

the gradients of the predicted score, s_c with respect to the elements of \mathbf{F}_n [23], as

$$\alpha_n^{c, Grad} = \sum_{i,j} \frac{\partial s_c}{\partial F_n(i, j)}, \quad (3)$$

where different from (2), s_c is a sparse vector whose elements are zeros except the c -th element, which is equal to S_c . However, the highlighted regions generated by Grad-CAM are usually much smaller than the object. To provide a precise highlighted region, some further modified CAMs are proposed, like Grad-CAM++[2]. A. Chattopadhyay et al proposed Grad-CAM++ which can produce more precise highlighted locality. Grad-CAM++ assumes different elements in the gradient matrix should have different contributions to features maps, thus an extra factor is introduced to realize this assumption using higher order partial gradient, as:

$$\alpha_n^{c, Grad++} = \frac{\frac{\partial^2 s_c}{\partial (F_n(i,j))^2}}{2 \frac{\partial^2 s_c}{\partial (F_n(i,j))^2} + \sum_{a,b} F_n(a, b) \frac{\partial^3 s_c}{\partial (F_n(i,j))^3}} \sum_{i,j} \frac{\partial s_c}{\partial F_n(i, j)}. \quad (4)$$

However, the gradient, $\frac{\partial s_c}{\partial F_n}$, is usually heavily noised or sometimes even all-zero. It is probably because 1) CNN is trained to learn a generalized capability to classify a general concept rather than a specific object. 2) some unreasonable phenomena emerged in CNN's training, like gradient vanishing and gradient exploding. D. Omeiza et al. proposed Smooth Grad-CAM++ to further suppress the noise. The weights of Smooth Grad-CAM++ are defined using the average of the gradients as:

$$\alpha_n^{c, SmoothGrad++} = \frac{\frac{1}{m} \sum_{m=1}^M D_1^n}{2 \frac{1}{m} \sum_{m=1}^M D_2^n + \sum_{a,b} F_n(a, b) \frac{1}{m} \sum_{m=1}^M D_3^n} \left(\frac{1}{m} \sum_{m=1}^M D_1^n \right) \quad (5)$$

where $D_1^n = \sum_{i,j} \frac{\partial s_c}{\partial F_n(i,j)}$, $D_2^n = \sum_{i,j} \frac{\partial^2 s_c}{\partial (F_n(i,j))^2}$, and $D_3^n = \sum_{i,j} \frac{\partial^3 s_c}{\partial (F_n(i,j))^3}$ when the input is added with random noise for M times (M is a constant integer). This smoothing strategy is intuitive but still rough for some complex CNN structures. To further enhance the interpretability of weights, R. Fu et al. proposed XGrad-CAM by introducing two completely explainable axioms to form the weight:

$$\alpha_n^{c, XGrad} = \sum_{i,j} \frac{F_n(i, j)}{\sum_{i,j} F_n(i, j)} \frac{\partial s_c}{\partial F_n(i, j)}. \quad (6)$$

Note neither Smooth Grad-CAM++ nor XGrad CAM can guarantee completely avoiding the above unreasonable phenomena in gradient computing.

2.2. Gradient-free Class Activation Mapping

Gradient-free CAM: To completely solve the problems resulting from gradient computing, some gradient-free CAMs

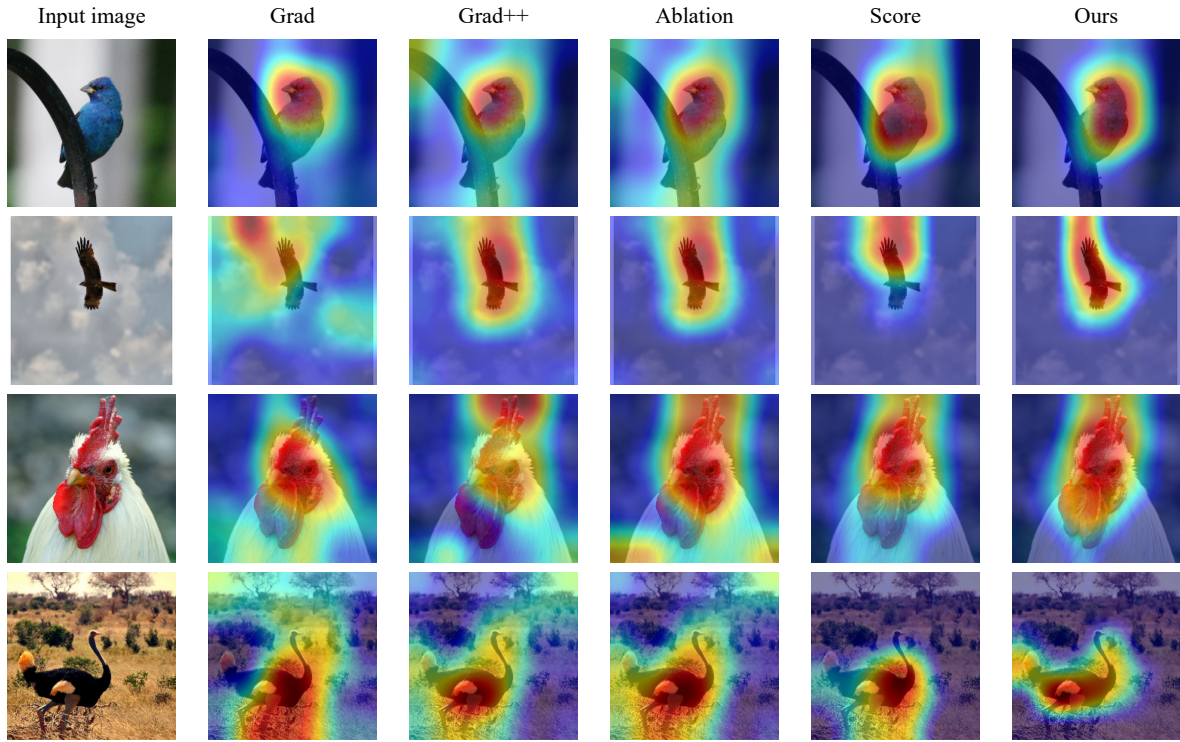


Figure 1: The heatmaps are produced by different CAMs. The first column is input images (indigo finch, eagle, rooster, and ostrich from top to bottom). The second to fifth columns are heatmaps produced by Grad-CAM, Grad-CAM++, Ablation-CAM, Score-CAM, and Cluster-CAM.

are proposed, i.e., Ablation-CAM [18] and Score-CAM [35], to form the weights using the impact of each feature map on the predicted score instead of using gradient. In Ablation-CAM, the weights are defined as:

$$\alpha_n^{c, Ablation} = \frac{S_c - S_{c,n}}{S_c}, \quad (7)$$

where $S_{c,n}$ denotes the predicted score for class c when n -th feature map is set to zero. In this case, a large weight will be assigned to the current feature map if the removal of it can lead to a dramatic drop in the predicted score ($S_c - S_{c,n}$ is a large value) and vice versa. The authors argue that Ablation-CAM is immune to both saturation which marks a filter as important although it is not important, and explosion which marks a filter that has a very small influence as having high importance. Different from Ablation-CAM, Score-CAM considers measuring the impact of the feature map by introducing the input image, \mathbf{X} , as

$$\alpha_n^{c, Score} = S_c(\mathbf{X} \circ \mathbf{H}_n) - S_c(\mathbf{X}_b) \quad (8)$$

$$\mathbf{H}_n = s(\text{Up}(\mathbf{F}_n)), \quad (9)$$

where \circ denotes the element-wise multiplication, \mathbf{X}_b is a baseline image which can be set the input image itself, $\text{Up}(\cdot)$ denotes the operation that upsamples \mathbf{F}_n into the input size and $s(\cdot)$ is a normalization function that maps each element in the input matrix into $[0, 1]$. $\mathbf{X} \circ \mathbf{H}_n$ can be deemed as filtering which only passes elements in \mathbf{X} masked by \mathbf{H}_n , thus

a large weight will be assigned if most target-discriminative are preserved by the current feature map, i.e. $f(\mathbf{X} \circ \mathbf{H}_n)$ is higher than $S_c(\mathbf{X}_b)$ and vice versa. Currently, gradient-free CAMs have drawn more attention than gradient-based CAMs due to their superior performance and explainable definition of weights. However, gradient-free CAMs are much more time-consuming than gradient-based CAMs because hundreds or even thousands of forward inference are required while those gradient-based CAMs only require one forward inference.

3. Methodology

In this section, we will first introduce some basic concepts on graph-based spectral clustering and K-means. Then we present the detailed procedures of Cluster-CAM.

3.1. Spectral Clustering and K-means

Spectral clustering is a widely-used unsupervised clustering algorithm based on graph signal processing [28, 29, 15, 22]. Specifically, the processed data (feature maps, \mathbf{F}_n) are regarded as vertices in a graph topology. Then the elements, $S(i, j)$, of the similarity matrix, \mathbf{S} , can be defined:

$$S(i, j) = \text{similarity}(\mathbf{F}_i, \mathbf{F}_j), \quad (10)$$

where $\text{similarity}(\cdot)$ refers to a function that measures the similarity between two vertices (feature maps). If we use the structural similarity index (SSIM), then it ranges from 0 (no

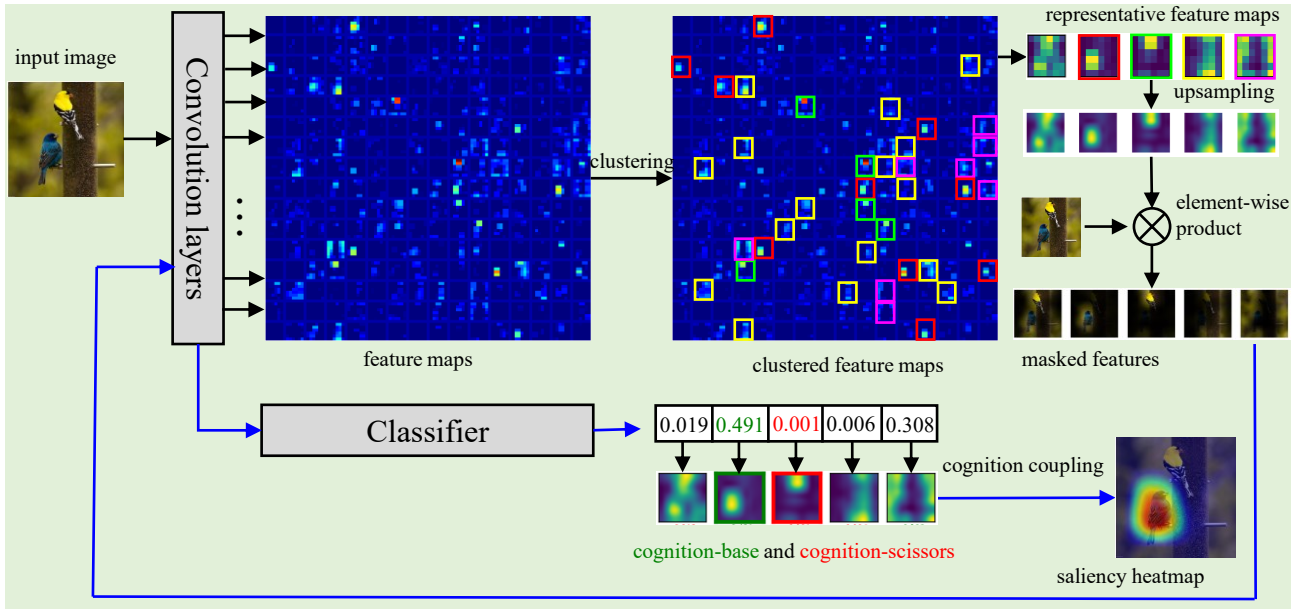


Figure 2: The flowchart of Cluster-CAM.

similarity) to 1 (identical feature maps). The elements of the weighted adjacency matrix, \mathbf{A} , can be defined as:

$$\begin{cases} A(i, j) = \exp(-(1 - S(i, j))/\sigma), & \text{if } S(i, j) > \theta, \\ A(i, j) = 0, & \text{else,} \end{cases} \quad (11)$$

where θ is a threshold to keep the direct edge in the corresponding graph for two neighboring vertices and σ is a parameter. Note that, by definition of similarity, this adjacency matrix is a symmetric matrix resulting in an undirected graph, that is, $A(i, j) = A(j, i)$.

The similarity can be defined using the difference between two vertices (feature maps), $d(i, j) = \|\mathbf{F}_i - \mathbf{F}_j\|$. Then the weighted adjacency matrix is defined by

$$\begin{cases} A(i, j) = \exp(-d^2(i, j)/\sigma^2), & \text{if } S(i, j) > \theta, \\ A(i, j) = 0, & \text{else,} \end{cases} \quad (12)$$

where θ and σ have the same role as in (11).

In order to produce the vectors for spectral clustering, now we continue and compute the graph Laplacian matrix, \mathbf{L} , as

$$\mathbf{L} = \mathbf{D} - \mathbf{A} \quad (13)$$

where $D(i, i) = \sum_j A(i, j)$ are the elements of the degree matrix \mathbf{D} which is diagonal.

In practice, the graph Laplacian matrix usually can be normalized, as

$$\mathbf{L}_N = \mathbf{D}^{-\frac{1}{2}} \mathbf{L} \mathbf{D}^{-\frac{1}{2}} = \mathbf{I} - \mathbf{D}^{-\frac{1}{2}} \mathbf{A} \mathbf{D}^{-\frac{1}{2}}. \quad (14)$$

The clustering results obtained using these two matrices are very similar.

The eigendecomposition of the graph Laplacian

$$\mathbf{L} = \mathbf{U}^T \mathbf{\Lambda} \mathbf{U}. \quad (15)$$

Results in eigenvectors $\mathbf{u}_1, \mathbf{u}_2, \dots, \mathbf{u}_N$ that are the columns of matrix \mathbf{U} . The smoothness index of these vectors is equal to the corresponding eigenvalue λ_i . In clustering the data into two clusters only the eigenvector \mathbf{u}_2 is used (Fiedler vector) since the vector \mathbf{u}_1 is omitted as its elements are constant.

If we want to get a few clusters (Q clusters) then we can use K the smoothest eigenvectors, $\mathbf{u}_2, \mathbf{u}_3, \dots, \mathbf{u}_{K+1}$, written in the matrix form as

$$\mathbf{B} = [\mathbf{u}_2 \quad \mathbf{u}_3 \quad \dots \quad \mathbf{u}_{K+1}] = \begin{bmatrix} u_{12} & u_{13} & \dots & u_{1(K+1)} \\ u_{22} & u_{23} & \dots & u_{2(K+1)} \\ \vdots & \vdots & \ddots & \vdots \\ u_{N2} & u_{N3} & \dots & u_{N(K+1)} \end{bmatrix}, \quad (16)$$

where N features with K dimension are considered.

The clusters are determined based on the K -dimensional spectral similarity vectors, $\mathbf{q}_1 = [u_{12}, u_{13}, \dots, u_{1(K+1)}]$, $\mathbf{q}_2 = [u_{22}, u_{23}, \dots, u_{2(K+1)}]$, ..., $\mathbf{q}_N = [u_{N2}, u_{N3}, \dots, u_{N(K+1)}]$, defined for vertices (features $\mathbf{F}_1, \mathbf{F}_2, \dots, \mathbf{F}_N$).

In this way, the dimension of the measuring distance is significantly reduced from the original N dimensional space in $d(i, j) = \|\mathbf{F}_i - \mathbf{F}_j\|$ to a very low K -dimensional spaces of spectral vectors \mathbf{q}_n .

Finally, the clustering result (the data grouped into Q clusters) can be refined using K-means and the Euclidean distance $d(i, j) = \|\mathbf{F}_i - \mathbf{F}_j\|$.

Note that the traditional K-means algorithm can be used with an initial random clustering of feature maps into Q clusters, with a slower convergence due to random initialization. In this case, all the feature maps are grouped into Q initial

clusters, \mathbb{Q}_q , $q = 1, 2, \dots, Q$. Means of the feature maps are calculated for each cluster, $M_q = \text{mean}(\mathbf{F}_n, n \in \mathbb{Q}_q)$. The distance of each feature map is checked with respect to each of the mean M_q . The feature map is reassigned to the cluster whose mean is the closest to the considered feature map. After all feature maps are considered, the means are recalculated for the new clusters. The procedure is repeated until no feature map changes its cluster.

3.2. Cluster-CAM

Now we are ready to introduce spectral clustering and K-means in Cluster-CAM. Here the feature maps, \mathbf{F} , represent the vertices in (10). Take Euclidean distance as similarity measurement, (10) can be expressed as:

$$S(i, j) = \exp\{-\|\mathbf{F}_i - \mathbf{F}_j\|\}, \quad (17)$$

where a shorter distance means a higher similarity. By substituting (17) into (11), (13), (14), and (16), we can split N feature maps into Q clusters, \mathbb{Q}_q , $q = 1, 2, \dots, Q$, $Q \ll N$. Then we can obtain the Q representative feature maps, $\tilde{\mathbf{F}} = [\tilde{\mathbf{F}}_1, \tilde{\mathbf{F}}_2, \dots, \tilde{\mathbf{F}}_Q]$, by calculating the mean of feature maps in each cluster, as

$$\tilde{\mathbf{F}}_q = \text{mean}\{\mathbf{F}_n, n \in \mathbb{Q}_q\}, \quad q = 1, \dots, Q. \quad (18)$$

Next we obtain the Hadamard product of $\tilde{\mathbf{F}}$ and \mathbf{X} ($\tilde{\mathbf{F}}$ will be upsampled to the same size of \mathbf{X}). This processing can be deemed as filtering that mainly passes those elements corresponding to large values in $\tilde{\mathbf{F}}$. The predicted score of each masked image is computed as:

$$\begin{aligned} \mathbf{y} &= [y_1, y_2, \dots, y_Q]^T \\ &= [S_{c,1}(\tilde{\mathbf{F}}_1 \circ \mathbf{X}), \dots, S_{c,Q}(\tilde{\mathbf{F}}_Q \circ \mathbf{X})]. \end{aligned} \quad (19)$$

In this case, we can obtain the cognition-base map and cognition scissors as

$$\tilde{\mathbf{F}}_{\text{base}} = \mathbf{F}_{q_{\max}}, \quad q_{\max} = \arg \max_q(\mathbf{y}) \quad (20)$$

$$\tilde{\mathbf{F}}_{\text{scissors}} = \mathbf{F}_{q_{\min}}, \quad q_{\min} = \arg \min_q(\mathbf{y}). \quad (21)$$

Next, we can semantically couple the cognition-base map and cognition-scissors to form the salience heatmap, as:

$$\mathbf{H}^{\text{Cluster}} = \beta \tilde{\mathbf{F}}_{\text{base}} - (1 - \beta) \tilde{\mathbf{F}}_{\text{scissors}}, \quad (22)$$

where $\beta \in [0, 1]$ is a balance factor to adjust the importance of cognition-base map and cognition-scissors.

4. Experiments

In this section, we will present and analyze the performance of Cluster-CAM from various perspectives. Firstly we will briefly describe the dataset used in our experiments. Then we verify the superiority of Cluster-CAM to other existing CAMs.

4.1. Experimental Setup

Dataset: In the following experiments, CNNs are trained on a prevalent benchmark, i.e., ILSVRC [4]. In ILSVRC, there are around 1.2 million images with 1000 categories for training, and 50 thousand images with 1000 categories for validation.

Network Structure: In this paper, several classic CNNs, AlexNet [9] and VGG-16 [25], are used as classification models. Alex-Net is proposed by A. Krizhevsky et al., which consists of 5 convolutional units (a stack of convolutional layers, ReLU, and max pooling) and 3 fully-connected layers. VGG-16 is a very deep CNN with 13 convolutional layers and 3 fully-connected layers. VGG-16 has approximately 134M trainable parameters regardless of the output layer.

4.2. Performance of Discriminative Localization

Fig. 1 shows the salience heatmaps of different input images (indigo finch, eagle, rooster, and ostrich) by Grad-CAM, Grad-CAM++, Ablation-CAM, Score-CAM, and Cluster CAM. Visually, in comparison to existing CAMs, the highlighted region produced by Cluster-CAM mostly matches human's intuitive understanding of the discriminative part of the specific object. Take the indigo finch as an example, Grad-CAM only highlights the head of the bird, whereas Grad-CAM++ and Ablation-CAM highlight the complete finch but the branch (object-irrelevant information) is also included. Score-CAM and Cluster-CAM highlight the finch body without the branch. But obviously, the region produced by Cluster-CAM matches the profile of the finch more precisely than Score-CAM.

4.3. CNN's Cognitive Explanation

Cognition Analysis of Multi-objects Images: Images of multiple objects are optimal samples to verify the rationality of the cognition-base map and semantic-scissors in (20) and (21). As we discussed in Section 3, a reasonable cognition-base map should incorporate the object-relevant information as much as possible, while the corresponding cognition-scissors should include such information as less as better. Therefore, it is necessary to check whether the cognition-base map and cognition-scissors can interchange a multi-objects image if the target class is changed to another object. Fig. 3 shows the cognition-base map and cognition-scissors of two multi-objects images as well as the corresponding masked images. There are two types of dogs in the first image, i.e. elkhound (the big gray dog on the left) and spaniel (the tiny brown dog on the right). If the target class is elkhound, the third and the fourth clustered feature map are cognition-base map and cognition-scissors, respectively (marked by green and red squares). It matches human's cognition because cognition-base map incorporates both objects and cognition-scissors only selects the spaniel, thus the highlighted region will only be concentrated on the elkhound, as shown in the first row in the top-left subfigure in Fig. 3. When the target class is changed to the spaniel, the cognition-base map and cognition-scissors are also interchanged, as shown in the third row in the top-right subfigure in Fig. 3. The same phenomenon also emerges in indigo finch and goldfinch,

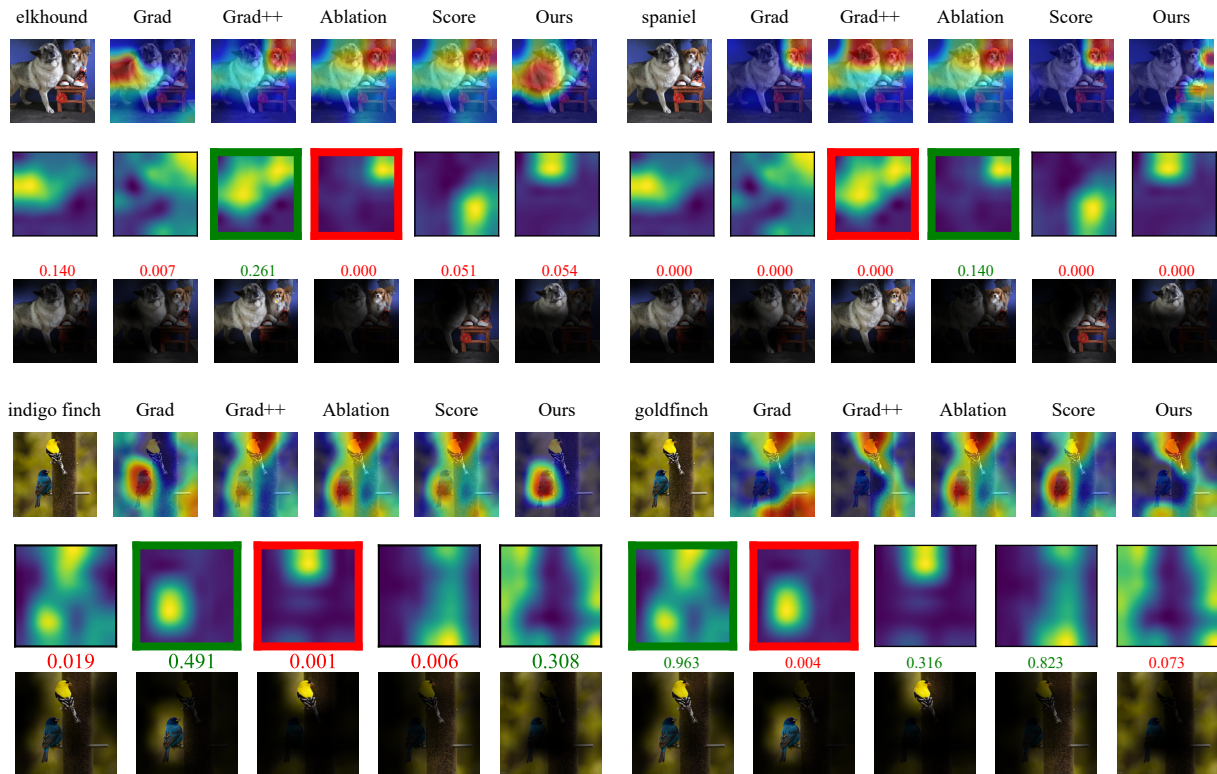


Figure 3: The analysis of feature maps for images of multiple objects. The heatmaps produced by different CAMs for the target label elkhound (first row in the top-left subfigure). The clustered feature maps (the second row in the top-left subfigure) and corresponding masked images (the third row in the top-left subfigure). Note that the cognition-base map and cognition-scissors are marked by green and red squares, respectively. The predicted score for the current class is provided above each masked image. The results with the target label spaniel are organized in the same structure (top-right subfigure). The indigo finch and goldfinch are shown in the bottom-left and bottom-right subfigures, respectively.

as shown in the bottom subfigures in Fig. 3. In this case, Cluster-CAM provides solid evidence that CNN’s recognition mechanism is similar to human cognition in multiple objects classification.

Cognition Analysis of Fine-grained Images: To further understand how CNN utilizes the learned information to make decisions, we can use CAM to interpret CNNs in fine-grained image classification. Fine-grained classification aims to distinguish subordinate categories within entry-level categories. Examples include recognizing species of birds such as northern cardinal or indigo bunting; monkeys such as guenon or langur. Fine-grained classification often requires much more detailed information compared with generic object recognition, like the texture of the skin, the thickness of the fur, etc, so CAMs on fine-grained images can tell whether the information is reasonably learned by CNN for classification. Fig. 4 shows the heatmaps generated by several mentioned CAMs given the input image of a guenon in the first row. Interestingly, they focus on completely different parts of the guenon. Grad-CAM and Grad-CAM++ highlight the guenon’s eyes and cheek, respectively. Ablation-CAM and Score-CAM both highlight the guenon’s face, whereas Cluster-CAM only

highlights the guenon’s forehead. Intuitively, Ablation-CAM and Score-CAM seem the most reasonable but the cognition-base map and cognition-scissors clearly show that the forehead is the most discriminative part but the face is negative for guenon’s classification. It will be understood if we further study the difference in species between guenon and langur. Guenon (widely distributed in Africa) is characterized by blond hair on the forehead and a busty white lip, whereas, langur (distributed in Asia) is characterized by a completely black face. We mark their characteristics by green and red circles in the third row in Fig. 4. It is the reason why the third feature map (face) is deemed as cognition-scissors, i.e., the black face is an interference factor for guenon’s categorizing. This example perfectly demonstrates the rationality of Cluster-CAM, particularly the cognition-scissors.

4.4. Ablation Study

Analysis of Different Layers: Most CNNs are constructed by a cascade of convolutional blocks (a block consists of convolutional layers, nonlinear activation, pooling operation, etc.). Fig. 5 shows the saliency heatmaps of different convolutional blocks in VGG-16. The results basically match

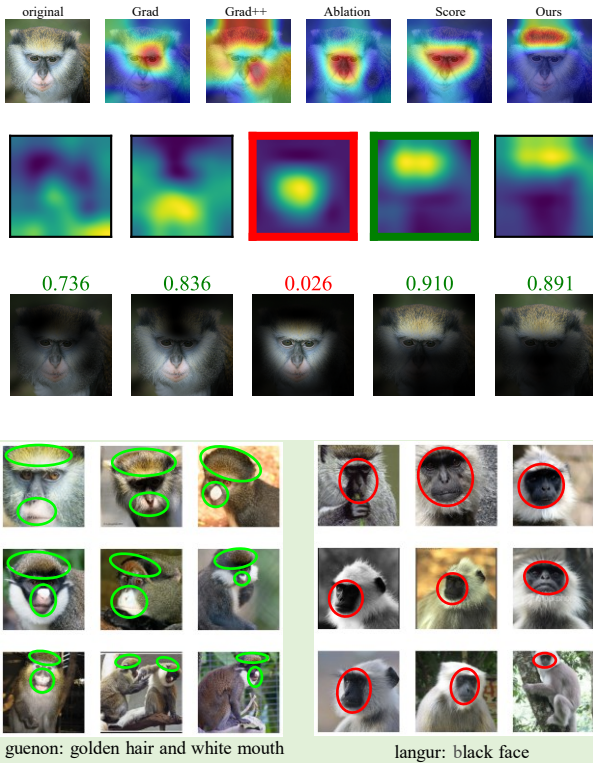


Figure 4: The cognition-base map (green square) and cognition-scissors (red square) in merged feature maps (top). The images are masked by corresponding feature masks as well as the predicted score (middle). Nine images of guenon and nine images of langur (bottom). Note that the discriminative characteristics of guenon (golden hair and white mouth) and langur (black face) are labeled with green and red circles, respectively.

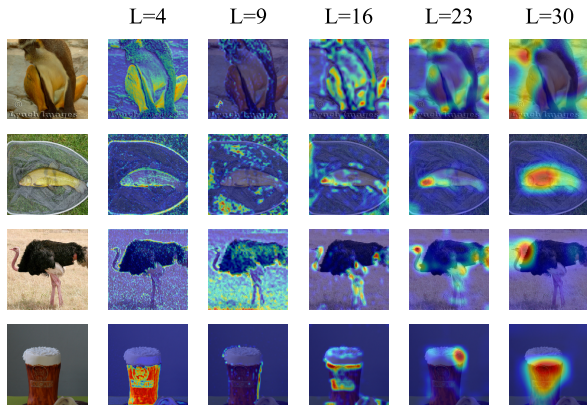


Figure 5: The heatmaps produced by Cluster-CAM with different numbers of clusters for VGG-16. L refers to the indices of layers in VGG-16.

human’s intuition that the shallow layers mainly capture some detailed information (e.g., texture and edge), whereas deep layers concentrate on those parts with clearer semantics.

Number of Clusters and CNN Structures: The number of clusters usually plays a critical role in clustering algorithms. Here we vary the cluster number from 2 to 8 and present the corresponding saliency heatmaps for AlexNet and VGG-16

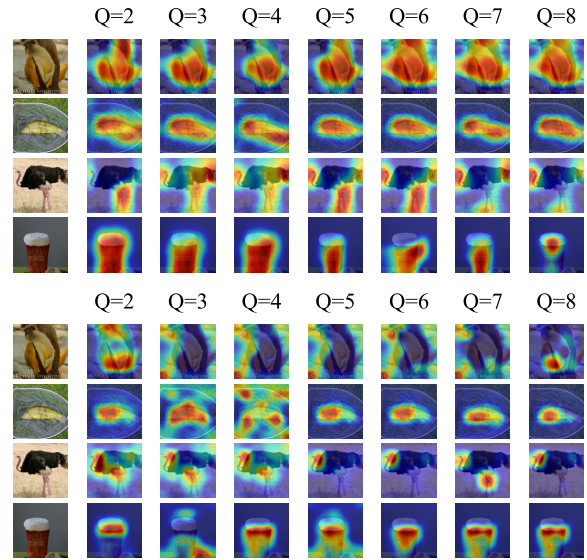


Figure 6: The heatmaps produced by Cluster-CAM (K-means) with different numbers of clusters for AlexNet (top) and VGG-16(bottom).

in Fig. 6. It shows the saliency heatmaps are sensitive to the number of clusters and are different with CNN models. For AlexNet, the highlighted region in heatmaps could be semantic chaos if the feature maps are split into too many or too few clusters. It is probably because a large number of clusters may introduce too many detailed patterns of the object and a small number of clusters may directly include background information. Therefore, the number of clusters should be selected as a median value. Note it is only an empirical conclusion and exclusion exists that the optimal value is 2 for the fourth row (beer) in Fig.6. It is probably because the object is simple and in regular shape, thus only two clusters are enough to represent all necessary information. For VGG-16, the highlighted region is more concentrated on a specific part of the object than AlexNet. It is probably because more detailed discriminative information could be captured in VGG-16 which has much deeper layers than AlexNet.

Clustering Method: In Section 3, we introduced two clustering algorithms, i.e., K-means and spectral clustering. Here we take each feature map as a vertex in the graph and use distance to construct the similarity matrix, adjacent matrix, degree matrix, and Laplacian matrix using (17), (10), (11), and (14). Fig. 7 shows the saliency heatmaps produced by spectral clustering with different clusters and different eigenvectors. It can be observed that the heatmaps are highly related to the number of eigenvectors rather than the clusters. Note that the optimal number of eigenvectors is highly related to the image itself, thus careful manipulation of this parameter is required for different objects to obtain the best heatmap. Therefore we will only use K-means to compute the qualitative evaluation metrics in the next section.

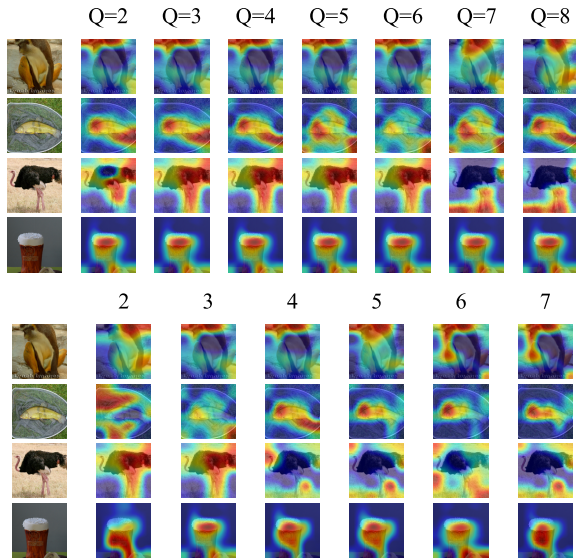


Figure 7: The heatmaps produced by Cluster-CAM with different numbers of clusters by spectral clustering (top) and heatmaps produced by Cluster-CAM with different numbers of eigenvectors (bottom).

4.5. Qualitative Evaluation

4.5.1. Performance Evaluation

To further evaluate the interpreting performance of Cluster-CAM quantitatively, two widely-used evaluation metrics are adopted in this paper, i.e., confidence drop and increase number [36, 41]. First of all, let's think about what kind of heatmap can be regarded as a good interpretation of CNN. A natural and intuitive idea is to measure how much the confidence (predicted score) of the target class will drop when the original image is partly occluded according to the heatmap. Specifically, for each image, a corresponding explanation map \mathbf{L}_c is generated by element-wise multiplication of the heatmaps and the current image as in (9) and (8).

Confidence drop: This metric compares the average drop of the model's confidence for a particular class in an image after occlusion as:

$$\text{confidence_drop} = \frac{S_c(\mathbf{X}) - S_c(\mathbf{X} \circ \mathbf{H}_n)}{S_c(\mathbf{X})}, \quad (23)$$

For example, assume that CNN predicts an object indigo finch in an image \mathbf{X} with confidence 0.8. When we input the explanation map, $\mathbf{X} \circ \mathbf{H}$, of this image, the CNN's confidence in the class indigo finch falls to 0.6. Then the confidence_drop would be 25%. It means that the most discriminative part (75%) is included in the highlighted region. Confidence drop is expected to be lower for a better CAM and is usually averaged over many images.

Increase number measures how many times the CNN's prediction score for c increased when the masked image is input. Specifically, it happens sometimes that the object is completely included and interference parts are occluded (e.g., the object-irrelevant parts and background) in the highlighted region. In this case, there will be an increase in the CNN's

Table 1

Performance Evaluation Metrics.

Method	Confidence drop ↓	Increase number ↑
Grad-CAM	17.94	19.15
Grad-CAM++	18.44	19.75
Ablation-CAM	12.38	24.67
Score-CAM	12.21	25.48
Cluster-CAM	11.60	26.10

Table 2

Efficiency Evaluation Metrics. Here $Q = 6$ in Cluster-CAM.

Method	Computing time ↓	number of FP ↓
Grad-CAM	0.078	1
Grad-CAM++	0.141	1
Ablation-CAM	2.206	256
Score-CAM	4.647	256
Cluster-CAM	0.382	6

predicted score for the class (i.e., confidence drop < 0). This value is computed as a percentage through the whole dataset.

Table 1 shows two evaluation metrics of the entire validation set in ILSVRC dataset (↓ means the lower value is better and ↑ means the higher value is better). These two metrics clearly demonstrate the superiority of Cluster-CAM to other existing CAMs. The metrics are computed in Pytorch 1.8.0+cu11.1, NVIDIA RTX-3070.

4.5.2. Efficiency Evaluation

Here we present two efficiency metrics, i.e., the average computing time and the number of forward propagation (FP) per image in Table 2. It is clear that Cluster-CAM greatly reduces the number of FP compared with Ablation-CAM and Score-CAM. Naturally, a significant improvement in efficiency emerges from Cluster-CAM, i.e., Cluster-CAM is 5.7 times faster than Ablation-CAM and 12.1 times faster than Score-CAM. Therefore, Cluster-CAM can obtain better visualization and interpretation performance than gradient-based and gradient-free CAMs with efficiency closer to gradient-based CAMs.

5. Conclusion

In this paper, we proposed Cluster-CAM, an effective and efficient CNN interpretation technique based on unsupervised clustering algorithms. Cluster-CAM is the first attempt to comprehensively analyze how to split feature maps into different groups and provide an artful strategy to remove the object-irrelevant elements by defining cognition-scissors. In Cluster-CAM, only several times of forward propagation is required per image while it is usually more than hundreds for other gradient-free CAMs. Qualitative and quantitative experimental results verified Cluster-CAM can obtain even better performance than gradient-free CAMs with much lower computing time.

Data Availability Statements

ILSVRC dataset can be downloaded from the website <https://www.image-net.org/challenges/LSVRC/>.

Acknowledgments

This work is funded by the National Natural Science Foundation of China (Grant No. 62276204, 61871301, 62071349), Project 2021ZDZX-GY-0001, science and technology project of Xianyang city.

References

- [1] Cao, J., Pang, Y., Han, J., Li, X., 2019. Hierarchical shot detector, in: Proceedings of the IEEE/CVF international conference on computer vision, pp. 9705–9714.
- [2] Chattopadhyay, A., Sarkar, A., Howlader, P., Balasubramanian, V.N., 2018. Grad-CAM++: Generalized gradient-based visual explanations for deep convolutional networks, in: In Proceedings of 2018 IEEE Winter Conference on Applications of Computer Vision (WACV), IEEE. pp. 839–847.
- [3] Chen, H., Jin, Y., Jin, G., Zhu, C., Chen, E., 2022. Semisupervised semantic segmentation by improving prediction confidence. IEEE Transactions on Neural Networks and Learning Systems 33, 4991–5003. doi:[10.1109/TNNLS.2021.3066850](https://doi.org/10.1109/TNNLS.2021.3066850).
- [4] Deng, J., Dong, W., Socher, R., Li, L.J., Li, K., Fei-Fei, L., 2009. Imagenet: A large-scale hierarchical image database, in: In proceedings of 2009 IEEE Conference on Computer Vision and Pattern Recognition (CVPR), pp. 248–255. doi:[10.1109/CVPR.2009.5206848](https://doi.org/10.1109/CVPR.2009.5206848).
- [5] Feng, Z., Ji, H., Stanković, L., Fan, J., Zhu, M., 2021a. SC-SM CAM: An efficient visual interpretation of CNN for SAR images target recognition. Remote Sensing 13, 4139.
- [6] Feng, Z., Zhu, M., Stanković, L., Ji, H., 2021b. Self-matching CAM: A novel accurate visual explanation of CNNs for SAR image interpretation. Remote Sensing 13, 1772.
- [7] Fu, R., Hu, Q., Dong, X., Guo, Y., Gao, Y., Li, B., 2020. Axiom-based Grad-CAM: Towards accurate visualization and explanation of CNNs, in: In Proceedings of the 2020 British Machine Vision Conference (BMVC 2020).
- [8] He, K., Zhang, X., Ren, S., Sun, J., 2016. Deep residual learning for image recognition, in: In Proceedings of 2016 IEEE conference on Computer Vision and Pattern Recognition (CVPR), pp. 770–778. doi:[10.1109/CVPR.2016.90](https://doi.org/10.1109/CVPR.2016.90).
- [9] Krizhevsky, A., Sutskever, I., Hinton, G.E., 2012. Imagenet classification with deep convolutional neural networks, in: Pereira, F., Burges, C., Bottou, L., Weinberger, K. (Eds.), Advances in Neural Information Processing Systems, Curran Associates, Inc.
- [10] Lapuschkin, S., Wäldchen, S., Binder, A., Montavon, G., Samek, W., Müller, K.R., 2019. Unmasking clever hans predictors and assessing what machines really learn. Nature communications 10, 1–8.
- [11] Liang, X., Hu, Z., Zhang, H., Lin, L., Xing, E.P., 2018. Symbolic graph reasoning meets convolutions. Advances in Neural Information Processing Systems 31.
- [12] Liu, J., Zhang, F., Zhou, Z., Wang, J., 2023. Bfmnet: Bilateral feature fusion network with multi-scale context aggregation for real-time semantic segmentation. Neurocomputing 521, 27–40. doi:<https://doi.org/10.1016/j.neucom.2022.11.084>.
- [13] Liu, K., Meng, R., Li, L., Mao, J., Chen, H., 2022a. Sisl-net: Saliency-guided self-supervised learning network for image classification. Neurocomputing 510, 193–202. doi:<https://doi.org/10.1016/j.neucom.2022.09.029>.
- [14] Liu, Z., Mao, H., Wu, C.Y., Feichtenhofer, C., Darrell, T., Xie, S., 2022b. A convnet for the 2020s, in: In Proceedings of the IEEE/CVF Conference on Computer Vision and Pattern Recognition (CVPR), pp. 11976–11986.
- [15] Ma, X., Zhang, S., Pena-Pena, K., Arce, G.R., 2021. Fast spectral clustering method based on graph similarity matrix completion. Signal Processing 189, 108301. doi:<https://doi.org/10.1016/j.sigpro.2021.108301>.
- [16] Macpherson, T., Churchland, A., Sejnowski, T., DiCarlo, J., Kamitani, Y., Takahashi, H., Hikida, T., 2021. Natural and artificial intelligence: A brief introduction to the interplay between ai and neuroscience research. Neural Networks 144, 603–613. doi:<https://doi.org/10.1016/j.neunet.2021.09.018>.
- [17] Omeiza, D., Speakman, S., Cintas, C., Weldermariam, K., 2019. Smooth grad-cam++: An enhanced inference level visualization technique for deep convolutional neural network models. arXiv preprint arXiv:1908.01224 .
- [18] Ramaswamy, H.G., et al., 2020. Ablation-cam: Visual explanations for deep convolutional network via gradient-free localization, in: In Proceedings of the IEEE Winter Conference on Applications of Computer Vision (WACV), pp. 983–991.
- [19] Redmon, J., Divvala, S., Girshick, R., Farhadi, A., 2016. You only look once: Unified, real-time object detection, in: In Proceedings of 2016 IEEE Conference on Computer Vision and Pattern Recognition (CVPR), pp. 779–788. doi:[10.1109/CVPR.2016.91](https://doi.org/10.1109/CVPR.2016.91).
- [20] Ren, J., Li, M., Liu, Z., Zhang, Q., 2021. Interpreting and disentangling feature components of various complexity from DNNs, in: In proceedings of International Conference on Machine Learning, PMLR. pp. 8971–8981.
- [21] Saleem, R., Yuan, B., Kurugollu, F., Anjum, A., Liu, L., 2022. Explaining deep neural networks: A survey on the global interpretation methods. Neurocomputing 513, 165–180. doi:<https://doi.org/10.1016/j.neucom.2022.09.129>.
- [22] Scalzo, B., Stanković, L., Daković, M., Constantinides, A.G., Mandic, D.P., 2023. A class of doubly stochastic shift operators for random graph signals and their boundedness. Neural Networks 158, 83–88. doi:<https://doi.org/10.1016/j.neunet.2022.10.035>.
- [23] Selvaraju, R.R., Cogswell, M., Das, A., Vedantam, R., Parikh, D., Batra, D., 2017. Grad-CAM: Visual explanations from deep networks via gradient-based localization, in: In Proceedings of the 2017 IEEE international conference on computer vision, pp. 618–626.
- [24] Simonyan, K., Vedaldi, A., Zisserman, A., 2013. Deep inside convolutional networks: Visualising image classification models and saliency maps. arXiv preprint arXiv:1312.6034 .
- [25] Simonyan, K., Zisserman, A., 2015. Very deep convolutional networks for large-scale image recognition, in: 3rd International Conference on Learning Representations (ICLR 2015), pp. 1–14.
- [26] Spinelli, I., Scardapane, S., Uncini, A., 2022. A meta-learning approach for training explainable graph neural networks. IEEE Transactions on Neural Networks and Learning Systems , 1–9doi:[10.1109/TNNLS.2022.3171398](https://doi.org/10.1109/TNNLS.2022.3171398).
- [27] Srinivas, A., Lin, T.Y., Parmar, N., Shlens, J., Abbeel, P., Vaswani, A., 2021. Bottleneck transformers for visual recognition, in: In Proceedings of the IEEE/CVF Conference on Computer Vision and Pattern Recognition (CVPR), pp. 16519–16529.
- [28] Stankovic, L., Dakovic, M., Sejdic, E., 2017. Vertex-frequency analysis: A way to localize graph spectral components [lecture notes]. IEEE Signal Processing Magazine 34, 176–182. doi:[10.1109/MSP.2017.2696572](https://doi.org/10.1109/MSP.2017.2696572).
- [29] Stankovic, L., Mandic, D.P., Dakovic, M., Kisil, I., Sejdic, E., Constantinides, A.G., 2019. Understanding the basis of graph signal processing via an intuitive example-driven approach. IEEE Signal Processing Magazine 36, 133–145. doi:[10.1109/MSP.2019.2929832](https://doi.org/10.1109/MSP.2019.2929832).
- [30] Sun, S., Song, B., Cai, X., Du, X., Guizani, M., 2022. CAMA: Class activation mapping disruptive attack for deep neural networks. Neurocomputing 500, 989–1002. doi:<https://doi.org/10.1016/j.neucom.2022.05.065>.
- [31] Tan, R., Gao, L., Khan, N., Guan, L., 2022. Interpretable artificial intelligence through locality guided neural networks. Neural Networks 155, 58–73. doi:<https://doi.org/10.1016/j.neunet.2022.08.009>.
- [32] Townsend, J., Chaton, T., Monteiro, J.M., 2020. Extracting relational explanations from deep neural networks: A survey from a neural

symbolic perspective. *IEEE Transactions on Neural Networks and Learning Systems* 31, 3456–3470. doi:10.1109/TNNLS.2019.2944672.

- [33] Tu, Z., Zhou, A., Gan, C., Jiang, B., Hussain, A., Luo, B., 2021. A novel domain activation mapping-guided network (DA-GNT) for visual tracking. *Neurocomputing* 449, 443–454. doi:https://doi.org/10.1016/j.neucom.2021.03.056.
- [34] Vlahek, D., Mongus, D., 2021. An efficient iterative approach to explainable feature learning. *IEEE Transactions on Neural Networks and Learning Systems*, 1–13doi:10.1109/TNNLS.2021.3107049.
- [35] Wang, H., Wang, Z., Du, M., Yang, F., Zhang, Z., Ding, S., Mardziel, P., Hu, X., 2020. Score-CAM: Score-weighted visual explanations for convolutional neural networks, in: *In Proceedings of the IEEE Conference on Computer Vision and Pattern Recognition (CVPR) workshops*, pp. 24–25.
- [36] Zeiler, M.D., Fergus, R., 2014. Visualizing and understanding convolutional networks, in: *European conference on computer vision*, Springer. pp. 818–833.
- [37] Zhang, Q., Rao, L., Yang, Y., 2021. Group-CAM: Group score-weighted visual explanations for deep convolutional networks. *arXiv preprint arXiv:2103.13859*.
- [38] Zhao, Z., Xie, X., Wang, C., Liu, W., Shi, G., Du, J., 2019. Visualizing and understanding of learned compressive sensing with residual network. *Neurocomputing* 359, 185–198. doi:https://doi.org/10.1016/j.neucom.2019.05.043.
- [39] Zhou, B., Bau, D., Oliva, A., Torralba, A., 2019. Interpreting deep visual representations via network dissection. *IEEE Transactions on Pattern Analysis and Machine Intelligence* 41, 2131–2145. doi:10.1109/TPAMI.2018.2858759.
- [40] Zhou, B., Khosla, A., Lapedriza, A., Oliva, A., Torralba, A., 2016. Learning deep features for discriminative localization, in: *In Proceedings of the 2016 IEEE Conference on Computer Vision and Pattern Recognition (CVPR)*, pp. 2921–2929.
- [41] Zhou, K., Kainz, B., 2018. Efficient image evidence analysis of cnn classification results. *arXiv preprint arXiv:1801.01693*.
- [42] Zhu, M., Feng, Z., Stanković, L., Ding, L., Fan, J., Zhou, X., 2022. A probe-feature for specific emitter identification using axiom-based grad-cam. *Signal Processing*, 108685.
- [43] Zhu, Y., Zhao, C., Wang, J., Zhao, X., Wu, Y., Lu, H., 2017. Couplenet: Coupling global structure with local parts for object detection, in: *Proceedings of the IEEE international conference on computer vision*, pp. 4126–4134.



Zhenpeng Feng was born in Xianyang, Shaanxi, China in 1996. He received a B.E. degree in School of Electronic Engineering, Xidian University in 2019. He is currently a Ph.D. student in explainable artificial intelligence at School of Electronic Engineering, Xidian University. He is also a visiting student in the University of Montenegro, working with Prof. Ljubiša Stanković’s research team. His research interests include interpreting deep neural networks and signal processing.



Hongbing Ji received a B.S. degree in radar engineering, an M.S. degree in circuit, signals, and systems, and the Ph.D. degree in signal and information processing from Xidian University, Xi’an, China, in 1983, 1989, and 1999, respectively. He is currently a full professor at Xidian University and a senior member of IEEE. His research interests include pattern recognition, radar signal processing, and multi-sensor information fusion.



Miloš Daković was born in 1970 in Nikšić, Montenegro. He received a B.S. in 1996, an M.S. in 2001, and a Ph.D. in 2005, all in electrical engineering from the University of Montenegro. He is a full professor at the University of Montenegro. His research interests are in signal processing, time-frequency signal analysis, compressive sensing, radar signal processing, and graph signal processing.



Xiyang Cui was born in Handan, Hebei, China in 1997. He received the B.E. degree and M.E. degree in Electronic Information Engineering and Electrical Circuit System from School of Electronic Engineering, Xidian University in 2019 and 2021, respectively. He is currently an investigator of an electronic company and collaborates with Zhenpeng Feng and Prof. Ljubiša Stanković in scientific research. His research interests include electrical circuit design and image processing.



Mingzhe Zhu was born in China in 1982. He received a B.S. degree in signal and information processing, a Ph.D. degree in pattern recognition and intelligent system from Xidian University in 2004 and 2010, respectively. He is currently an associate professor at School of Electronic Engineering, Xidian University. His research interests include non-stationary signal processing, time-frequency analysis, and target recognition.



Ljubiša Stanković was born in Montenegro, 1960. He was at the Ruhr University Bochum, 1997–1999, supported by the AvH Foundation. Stanković was the Rector of the University of Montenegro 2003–2008, the Ambassador of Montenegro to the UK, 2011–2015, and a visiting academic to the Imperial College London, 2012–2013. He published almost 200 journal papers. He is a member of the National Academy of Science and Arts (CANU) and the Academia Europaea. Stanković won the Best paper award from the EURASIP in 2017 and the IEEE SPM Best Column Award for 2020. Stanković is a professor at the University of Montenegro and a Fellow of the IEEE.